Supplementary material

TiO_2 Nanoparticles Catalyze Oxidation of Huntingtin Exon 1-Derived Peptides Impeding Aggregation: a Quantitative NMR Study of Binding and Kinetics

Alberto Ceccon, Vitali Tugarinov* and G. Marius Clore*

Laboratory of Chemical Physics, National Institute of Diabetes and Digestive and Kidney Diseases, National Institutes, Maryland 20892-0520

Experimental and 4 supplementary figures

Experimental

Preparation and characterization of titanium dioxide nanoparticles. TiO_2 nanopowder (> 99.5%) was purchased from Sigma-Aldrich (catalog number 718467) and stored in the dark. A TiO_2 stock suspension (15 $g \cdot L^{-1}$, 20 ml) was obtained by dissolving the nanopowder in 25 mM HEPES buffer (pH 6.8), 5 mM citrate. Citric acid was added to the solution as adsorption of citrate on TiO_2 nanoparticles prevents their sedimentation at pH ≥ 6.[1] TiO_2 suspensions, divided into 5 ml aliquots, were vortexed briefly and sonicated for 60 minutes in an ultrasonic bath cleaner equipped with temperature controller (Elma P Series; frequency = 37 kHz at maximum power). The size distribution and ζ-potential of the TiO_2 nanoparticles were determined by dynamic light scattering (Zetasizer Nano ZS, Malvern Instruments UK) at 10 °C upon dilution of the samples to 5 $g \cdot L^{-1}$ and 0.5 $g \cdot L^{-1}$, respectively, with 25 mM HEPES Buffer (pH 6.8) and 5 mM citrate (Figure S1). Each measurement consisted of 20 runs, and experiments were carried out in triplicate. Sample preparation and characterization were carried out in the dark. TiO_2 suspensions were wrapped with aluminium foil and stored in the dark at room temperature.

UV illumination and measurement of TiO_2 nanoparticle photocatalytic activity. Irradiation of TiO_2 nanoparticles with UV light was carried out using a ChemiImager 5500 instrument (Alpha Innotech, USA) emitting at 365 nm. TiO_2 suspensions (15 $g \cdot L^{-1}$, 5 ml) were exposed to UV light for 3 hours and then stored immediately in the dark to prevent generation of reactive oxygen species due to visible light. The size distribution of TiO_2 nanoparticles was also verified after UV light exposure and no variation in the size distribution was observed. Reactive oxygen species generated by photo-catalysis during UV irradiation, specifically, hydroxyl radicals ($^{\bullet}OH$), superoxide anion radicals ($^{\bullet}O_2^-$) and hydrogen peroxide (H_2O_2), were detected using the terephthalic acid (TA), nitro blue tetrazolium (NBT) and Amplex Red (AR) assays, respectively.

Terephthalic acid (TA, 2 mM final concentration) was added to a 5 $g \cdot L^{-1}$ TiO_2 suspension, incubated for 1 h and subsequently exposed to UV light for 3 hours. The presence of $^{\bullet}OH$ in the supernatant was assessed by removing the TiO_2 nanoparticles (by centrifugation at 17,000 rpm for 15 minutes) from the solution (Figure S2A). The $^{\bullet}OH$ lifetime was checked by adding TA (2 mM final concentration) to a TiO_2 nanoparticle suspension immediately after UV exposure and to the supernatant collected in the same way as described before. All fluorescence measurements were carried out using an Infinite M200 Pro (Tecan, Switzerland) plate reader. Emission of the OH-oxidized product was measured between 350 and 600 nm with an excitation wavelength of 312 nm.

Nitro blue tetrazolium (NBT, 2 mM final concentration) was added to a 5 $g \cdot L^{-1}$ TiO_2 suspension before and after UV exposure and the supernatant fractions collected as described for the terephthalic acid assay. Oxidation of NBT by $^{\bullet}O_2^-$ results in the formation of insoluble formazan that decreases NBT absorbance; the generation of $^{\bullet}O_2^-$ is manifested by a reduction in absorbance at 259 nm (Figure S2B).

Quantitative evaluation of H_2O_2 in a suspension of TiO_2 nanoparticles was determined using the Amplex Red Assay (Thermo Fisher). Briefly, in the presence of peroxidase, Amplex Red reacts with hydrogen peroxide (1:1 mol/mol) to yield the red-fluorescent oxidation product, resorufin. Amplex Red and horseradish heroxidase (100 μM and 0.1 U/ml, respectively) were added to a 10-fold dilution of a 5 $g \cdot L^{-1}$ TiO_2 suspension (pre-exposed to UV light for 3 hours). The presence of H_2O_2 was verified by direct addition of Amplex Red and horseradish peroxidase to the nanoparticle suspension, while the presence of H_2O_2 in the supernatant was verified by addition of Amplex Red and horseradish peroxidase after complete removal of TiO_2 nanoparticles as described above. The generation of H_2O_2 from nanoparticles in the absence of UV light was also monitored by adding Amplex Red and horseradish peroxidase to the TiO_2 suspension/supernatant stored in the dark. A microplate reader was used to measure the emission of resorufin (between 560 and 660 nm) and excitation at 540 nm. The reactions were incubated for 30 min before measurement. The measurement of H_2O_2 concentration was calibrated by construction of standard curves using known H_2O_2 concentrations.

Expression and purification of htt^{NT} and $htt^{NT}Q_{10}$ peptides. The GB1- $htt^{NT}Q_n$ fusion proteins (n = 0 or 10, where n is the number of C-terminal poly-glutamine repeats) were expressed in *E. Coli* BL21 (DE3)

cells grown in M9 minimal medium containing $^{15}NH_4Cl$ as the sole nitrogen source. The $htt^{NT}Q_n$ peptides were cleaved from GB1 by overnight incubation with Factor Xa (New England Biolabs) and the GB1 tag subsequently removed by reverse phase high pressure liquid chromatography (HPLC) as described previously.[2] A disaggregation procedure involving dissolution of the peptides in a 1:1 (v/v) mixture of trifluoroacetic acid (TFA) and hexafluoroisopropanol (HFIP) was carried to ensure complete removal of any pre-existing aggregates that can seed further aggregation.[3] The TFA:HFIP solvent mixture was then removed at room temperature for 16 h under a stream of argon gas. The peptide film was then dissolved in 0.1 mM TFA prior to lyophilization. Completion of the cleavage reaction and the peptide identity were confirmed by liquid phase chromatography coupled with mass spectrometry (LC-MS).

Thioflavin T (Tht) assay. $htt^{NT}Q_{10}$ aggregation was monitored using a Tht assay as described previously.[2] Briefly, 25 μM $htt^{NT}Q_{10}$ was incubated with 25 μM Tht in a 96-well micro-titer plate. ThT emission spectra were obtained using an Infinite M200 Pro (Tecan, Switzerland) plate reader with an excitation wavelength of 440 nm and emission wavelengths from 460 to 550 nm. Measurements were averaged and the background fluorescence (25 μM ThT) subtracted. Between the measurements the plates were sealed with parafilm to prevent evaporation and incubated in the dark at 4 °C. The ThT assay could not be used to monitor the impact of TiO_2 NPs on aggregation of $htt^{NT}Q_{10}$ as (a) ThT binds to TiO_2 NPs resulting in an increase in fluorescence in the dark, and (b) H_2O_2 generated upon illumination of TiO_2 NPs quenches ThT fluorescence, presumably through oxidation of ThT.

Preparation of NMR samples. NMR samples were prepared by mixing ^{15}N-labeled peptides (at a final concentration of 300 μM) with 5 $g \cdot L^{-1}$ TiO_2 nanoparticles (where needed). An agarose solution was added to the protein or the protein/nanoparticle solution at a final concentration of 0.5 % (w/v) to prevent sedimentation of TiO_2 NPs.[4] The solution was transferred to a NMR tube and allowed to cool on ice for 10 min. All NMR samples were prepared in 25 mM HEPES buffer (pH 6.8), 5 mM citrate, and 10% D_2O/90% H_2O (v/v).

NMR measurements. All NMR experiments were recorded at 10 °C using Bruker Avance-III spectrometers, equipped with TCI triple resonance *z*-axis gradient cryogenic probes operating at ^1H Larmor frequencies of 800.13, 600.82, and 500.68 MHz. NMR spectra were processed using the nmrPipe/nmrDraw suite of programs.[5]

$htt^{NT}Q_{10}$ aggregation in the absence or presence of TiO_2 nanoparticles was monitored by the integrated intensity of the amide proton envelope obtained from the first t_1 increment of a ^1H-^{15}N heteronuclear single quantum coherence (HSQC) correlation spectrum (from 7.8 to 8.6 ppm). The integrated intensity of the amide envelope reports on the total concentration of NMR visible species comprising the sum of reduced and oxidized states of monomeric $htt^{NT}Q_{10}$; the aggregates are broadened beyond detection and are not visible in the NMR spectrum. To correct for sample preparation to sample preparation variations in the fraction of oxidized (aggregation-incompetent) httNTQ10 present at t = 0, the normalized intensity, $I_{norm}(t)$, is given by $[I(t) - I_{oxi}(0)]/ [I(0) - I_{oxi}(0)]$ where $I(0)$ and $I_{oxi}(0)$ are the total intensity and the contribution of the oxidized species to the total intensity of NMR visible species at $t = 0$, and $I(t)$ is the total intensity of NMR visible species at time t. The fraction oxidized $htt^{NT}Q_{10}$ at $t = 0$ was determined from the ratio of oxidized to reduced ^1H-^{15}N cross-peak intensities in the HSQC spectrum recorded at $t = 0$.

Quantitative evaluation of Met^7 oxidation of htt^{NT} as a function of time was obtained from 2D ^1H-^{15}N HSQC spectra monitoring the decrease/increase in cross-peak intensities of residues corresponding to the reduced/oxidized forms of the peptide, respectively. Chemical shift assignments of htt^{NT} and (Met^7O)-htt^{NT} were taken from our previously published data.[2]

On-resonance ^{15}N-$R_{1\rho}$ and R_1 measurements were carried out using the pulse schemes described previously.[6-7] For the $R_{1\rho}$ measurements a spin-lock field strength of 1.0 kHz was used to suppress chemical exchange. ^{15}N-R_2 values were extracted from the measured ^{15}N-$R_{1\rho}$ and R_1 values using the relationship $R_2 = (R_{1\rho} - R_1\cos^2\theta)/\sin^2\theta$, where θ is the angle subtended by the effective spin-lock field with respect to the external magnetic field. Lifetime line broadening, ^{15}N-ΔR_2, values were calculated as a difference between ^{15}N-R_2 values obtained in the presence and absence of TiO_2 nanoparticles.

2D ^{15}N-DEST measurements were performed at 600 MHz by applying a 0.7 s continuous wave (CW) saturation pulse at radiofrequency (RF) field strengths of 350, 500 and 750 Hz for htt^{NT}, and 500 and 750

MHz for (Met^{7}O)-htt^{NT}. The carrier frequency offsets in kHz were: -22.0, -20.0, -18.0, -16.0, -14.0, -12.0, -10.0, -8.0, -6.0, -5.0, -4.0, -3.0, -2.0, -1.0, -0.5, 0.0, 0.5, 1.0, 2.0, 3.0, 4.0, 5.0, 6.0, 8.0, 10.0, 12.0, 14.0, 16.0, 18.0, 20.0, 22.0. The carrier was set to 121.5 ppm for ^{15}N and 4.7 ppm for ^{1}H. All experiments were normalized to a reference experiment performed applying the same RF field strengths but with the offset moved to -1 MHz.

Kinetics of htt^{NT} oxidation by TiO_2 nanoparticles. The system of differential equations describing Scheme 1 (main text) was integrated numerically using a Runge-Kutta method implemented in MatLab's (MathWorks Inc. MA) ordinary differential equation solver, *ode45*, and non-linear best-fitting was performed using an in-house program with uncertainties in the values of the optimized parameters, corresponding to confidence intervals of ±1 standard deviation, determined from the variance-covariance matrix of the fit. The differential equations corresponding to Scheme 1 are as follows:

$$\begin{aligned} d[\mathrm{P_{red}}]/dt &= -[\mathrm{P_{red}}](k_{\mathrm{agg}} + k_3^{\mathrm{dark}} + k_1[\mathrm{H_2O_2}]_{\mathrm{UV}}^{\mathrm{sol}} + k_2[\mathrm{H_2O_2}]_{\mathrm{UV}}^{\mathrm{TiO_2}}) \\ d[\mathrm{P_{oxi}}]/dt &= [\mathrm{P_{red}}](k_3^{\mathrm{dark}} + k_1[\mathrm{H_2O_2}]_{\mathrm{UV}}^{\mathrm{sol}} + [\mathrm{H_2O_2}]_{\mathrm{UV}}^{\mathrm{TiO_2}}) \\ d[\mathrm{H_2O_2}]_{\mathrm{UV}}^{\mathrm{sol}}/dt &= -k_1[\mathrm{P_{red}}][\mathrm{H_2O_2}]_{\mathrm{UV}}^{\mathrm{sol}} \\ d[\mathrm{H_2O_2}]_{\mathrm{UV}}^{\mathrm{TiO_2}}/dt &= -k_2[\mathrm{P_{red}}][\mathrm{H_2O_2}]_{\mathrm{UV}}^{\mathrm{TiO_2}} \end{aligned} \quad \text{(S1)}$$

where $k_3^{\mathrm{dark}} = k_2[\mathrm{H_2O_2}]_{\mathrm{dark}}$, and $[\mathrm{H_2O_2}]_{\mathrm{dark}}$ is the steady-state level of H_2O_2 on the TiO_2 NPs in the dark.

k_1 was obtained by fitting the disappearance of reduced and appearance of oxidized htt^{NT} ^{1}H-^{15}N cross-peaks upon addition of 100 μM H_2O_2 to 300 μM htt^{NT} (see Figure 2B). k_2 was obtained by fitting the disappearance of reduced and appearance of oxidized htt^{NT} ^{1}H-^{15}N cross-peaks upon addition of 5g·L^{-1} TiO_2 NPs pre-exposed to UV irradiation for 3 hours to 300 μM htt^{NT} by setting k_1 to its previously determined value, and optimizing the value of k_2 (with $k_3^{\mathrm{dark}} = k_2[\mathrm{H_2O_2}]_{\mathrm{dark}}$ and $k_{\mathrm{agg}} = 0$). k_{agg} for htt^{NT}Q$_{10}$ in the absence of TiO_2 NPs was determined by fitting a single exponential decay to the normalized amide proton envelope intensity as a function of time. k_{agg} for htt^{NT}Q$_{10}$ in the presence of 5g·L^{-1} TiO_2 NPs (pre-exposed to UV irradiation for 3 hours) was determined by fitting the normalized amide proton envelope intensity (proportional to the sum of NMR visible reduced and oxidized monomeric states) as a function of time, integrating all the differential equations in Eq. S1 and optimizing the value of k_{agg}, with k_1, k_2 and k_3^{dark} (= $k_2[\mathrm{H_2O_2}]_{\mathrm{dark}}$) set to their previously determined values.

Simultaneous analysis of DEST and ΔR_2 data. Experimental ^{15}N-DEST and ^{15}N-ΔR_2 data obtained for htt^{NT} and (Met^{7}O)-htt^{NT} in the presence of TiO_2 nanoparticles were fit simultaneously by minimizing the following error function:

$$F = \alpha_1 \sum_i \left(\frac{\Delta R_{2,\mathrm{obs}}^i - \Delta R_{2,\mathrm{calc}}^i}{\sigma_{\Delta R_2}^i}\right)^2 + \alpha_2 \sum_i \sum_k \sum_{j=1}^{3(2)} \left(\frac{\kappa_{\mathrm{obs}}^{i,k,j} - \kappa_{\mathrm{calc}}^{i,k,j}}{\sigma_{\mathrm{K}}^i}\right)^2 \quad \text{(S2)}$$

where the first term relates to the ΔR_2 data and the second for the DEST normalized intensities, κ. The subscripts 'obs' and 'calc' refer to experimental and calculated values, respectively. The latter are obtained by propagation of the appropriate set of Bloch-McConnell equations for a three-state exchanging system.[8] i, j, k refer to residue number, DEST field strength and DEST offset, respectively; and α_1 and α_2 are empirically determined factors used to appropriately weight the different data types, and were set to values of 3 and 1, respectively. The set of global optimized parameters for the $\mathrm{P_F^{red}} \leftrightarrow \mathrm{P_R^{red}} \leftrightarrow \mathrm{P_B^{red}}$ and $\mathrm{P_F^{oxi}} \leftrightarrow \mathrm{P_R^{oxi}} \leftrightarrow \mathrm{P_B^{oxi}}$ pathways describing the behavior of the htt^{NT} core (residues 3-13) comprised $\{p_{\mathrm{R}}^{\mathrm{red}}, k_{\mathrm{FR}}, k_{\mathrm{RB}}, k_{\mathrm{BR}}\}$ and $\{p_{\mathrm{R}}^{\mathrm{oxi}}, k'_{\mathrm{FR}}, k'_{\mathrm{RB}}, k'_{\mathrm{BR}}\}$, respectively. A total of 8 and 4 residues were analyzed for htt^{NT} and (Met^{7}O)-htt^{NT}, respectively.

A different three-state exchange model ($\mathrm{P_F^{red}} \leftrightarrow \mathrm{P_R^{red}} \leftrightarrow \mathrm{P_T^{red}}$) was used for Leu^3 and three C-terminal residues (Lys^{14}, Ser^{15}, Phe^{16}) of htt^{NT} bearing in mind that the exchange process for these residues involves initial binding followed by reversible detachment from the nanoparticle surface (state $\mathrm{P_T^{red}}$ where the

subscript "T" denotes a "tethered" state). The set of global optimized parameters for the $P_F^{red} \leftrightarrow P_R^{red} \leftrightarrow P_T^{red}$ pathway comprised: $\{p_R^{red}, k_{FR,} k_{on}^{overall}, k_{off}^{overall}\}$, where $k_{on}^{overall}$ and $k_{off}^{overall}$ are the rate constants for the overall inter-conversion between P_R^{red} and P_T^{red} (see Figure 4 in the main text). The rate constants k_{BT} and k_{TB} for the exchange process between the nanoparticle-bound peptide (P_B^{red}) and the tethered state P_T^{red}, are given by $k_{on}^{overall} k_{BR}/(k_{RB} - k_{on}^{overall})$ and $k_{off}^{overall}\ (1 + k_{BT}/k_{BR})$, respectively.

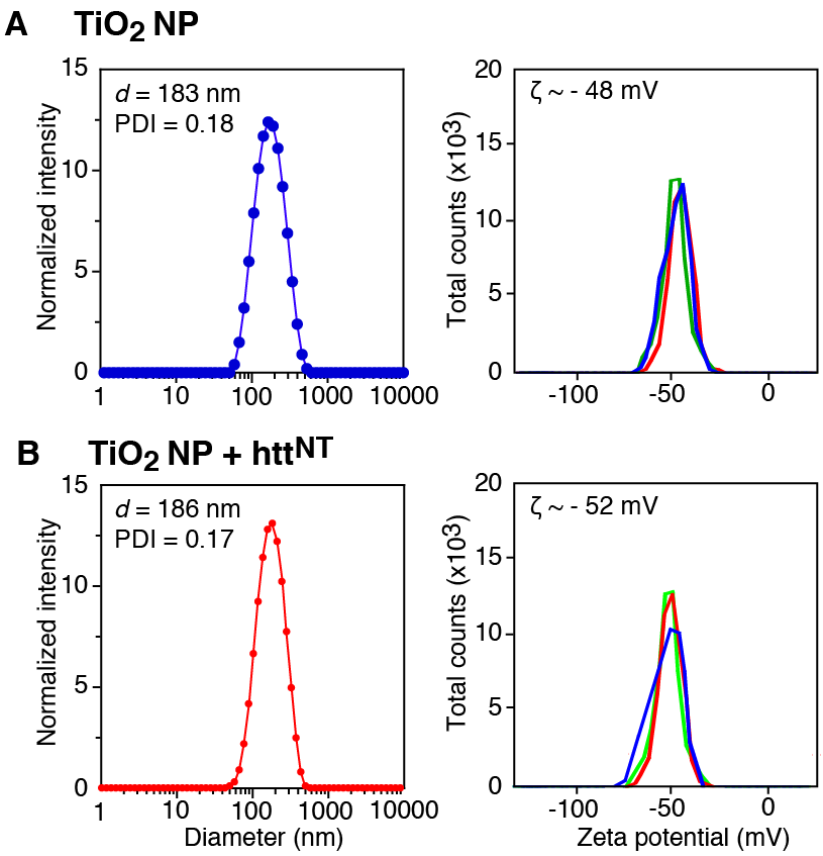

Figure S1. Characterization of citrate-coated TiO_2 nanoparticles in the (A) absence and (B) presence of 300 μM htt^{NT} by dynamic light scattering (DLS). The left panels show the intensity-weighted size distribution of TiO_2 nanoparticles. The right panels display the Zeta (ζ) potential distributions of TiO_2 nanoparticles determined using the Smoluchowski approximation for three consecutive measurements. Experiments were conducted on a 5 $g \cdot L^{-1}$ TiO_2 suspension in the presence of 5 mM citric acid at 10 °C. The values for the *z*-average particle diameter (as obtained from Cumulant analysis), the polydispersity index (PDI), and the ζ-potential are indicated.

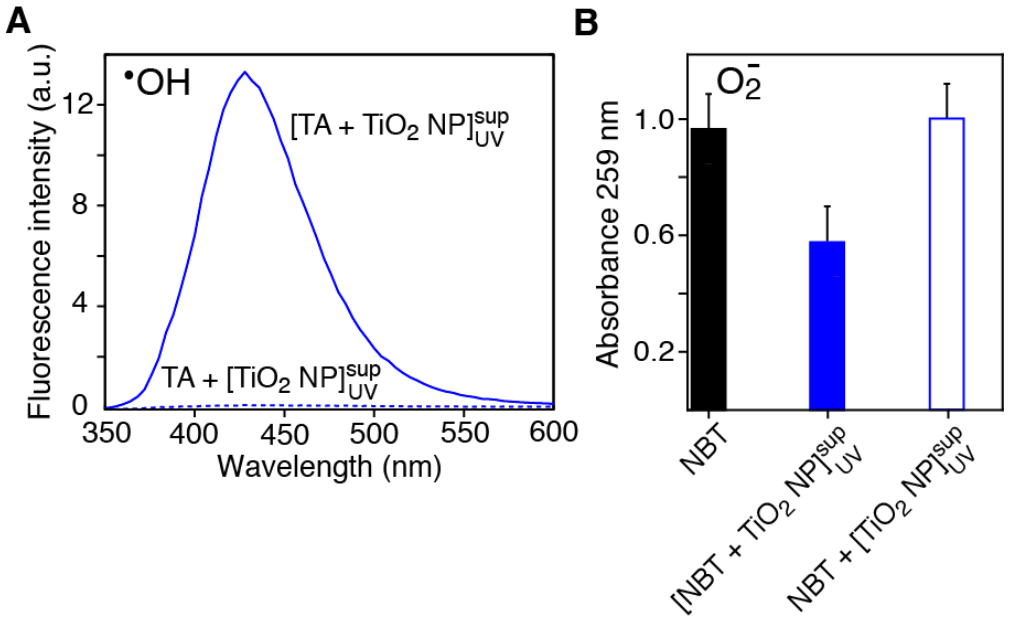

Figure S2. Evaluation of the life-time of reactive oxygen species generated by TiO_2 nanoparticles. (A) Fluorescent emission spectra of 2 mM terephthalic acid (TA), used to detected $^{\bullet}OH$ radicals, after exposure of a 5 $g{\cdot}L^{-1}$ TiO_2 nanoparticle suspension to UV light. The spectrum obtained on the samples where TA was added either before or after exposure of the TiO_2 nanoparticles to UV light are shown by the blue solid and dashed lines, respectively. (B) Absorbance at 259 nm of 2 mM Nitro blue tetrazolium (NBT), used to detect $^{\bullet}O_2^-$ radicals, after exposure of a 5 $g{\cdot}L^{-1}$ TiO_2 nanoparticle suspension to UV light. The absorbance of NBT alone is shown by the black bar; the absorbance of NBT when added to TiO_2 nanoparticles before or after exposure to UV light are shown as solid and open blue bars, respectively. (The superscript "sup" indicates the supernatant after removal of the TiO_2 nanoparticles by centrifugation).

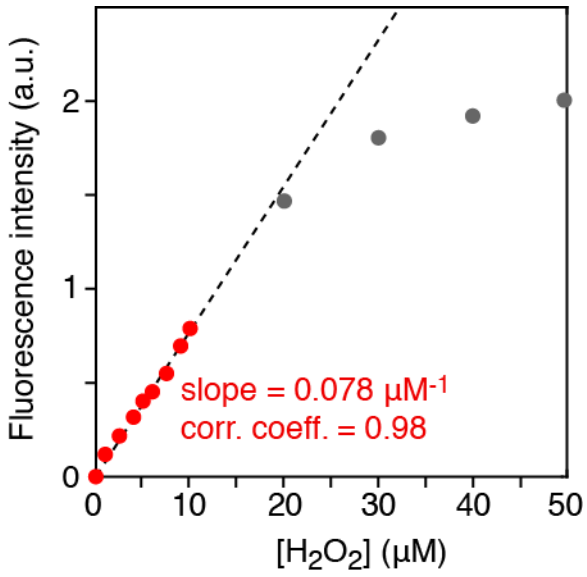

Figure S3. Standard calibration curve for the measurement of H_2O_2 concentration using the Amplex Red assay. Note the curve is only linear up to ~10 µM H_2O_2 (red circles), and hence care has to be taken to dilute samples prior to measurement to H_2O_2 concentrations at or below this level.

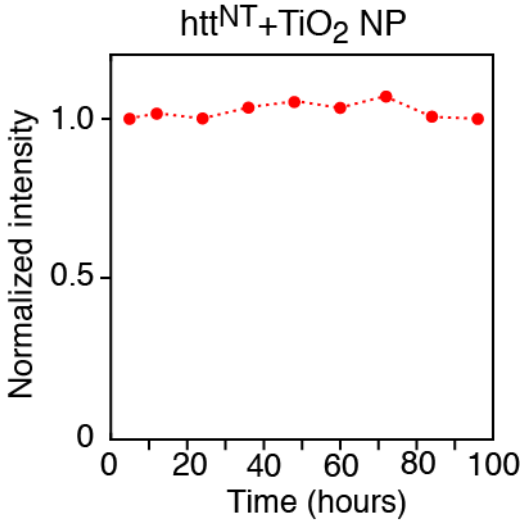

Figure S4. Stability of htt^{NT} in the presence of TiO_2 NPs. No change in the integrated intensity of the amide proton envelope is apparent over a period of 100 hours. Data were recorded on 300 μM htt^{NT} in the presence of 5 $g \cdot L^{-1}$ TiO_2 NPs.

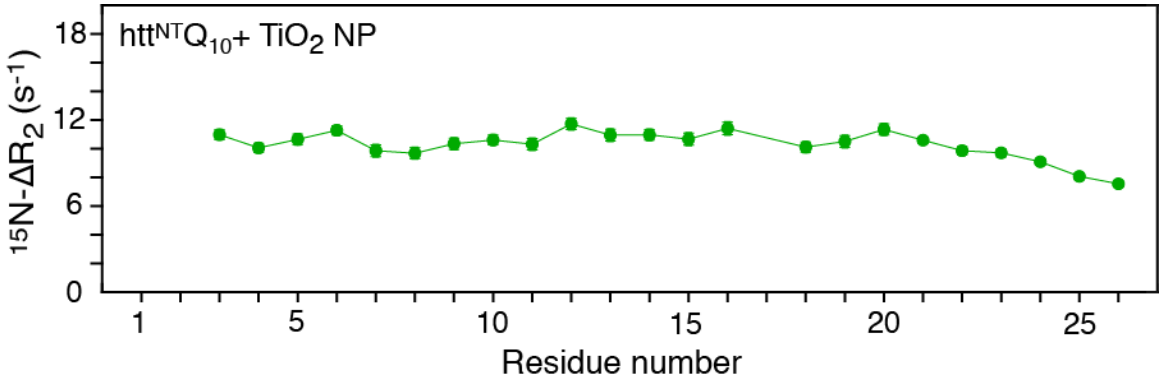

Figure S5. Binding of $htt^{NT}Q_{10}$ to TiO_2 NPs results in lifetime line broadening (^{15}N-ΔR_2) as a result of rapid decay of transverse relaxation in the TiO_2 NP-bound state. Data were acquired on 300 μM $htt^{NT}Q_{10}$ in the presence of 5 $g \cdot L^{-1}$ TiO_2 NPs in the dark.

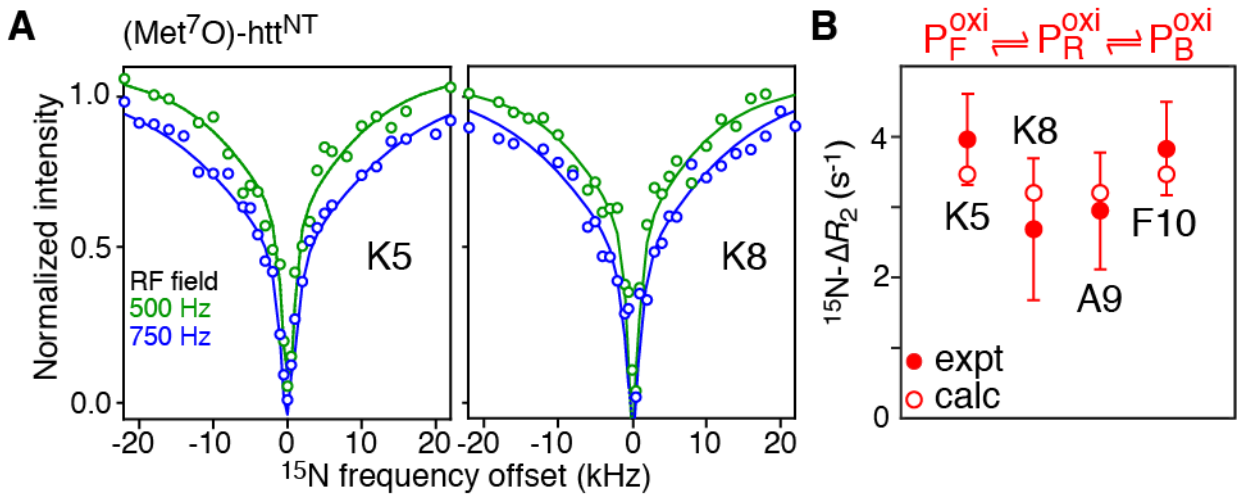

Figure S6. ^{15}N-DEST and ΔR_2 measurements on (Met^{7}O)-htt^{NT} in the presence of TiO_2 nanoparticles. (A) Representative experimental ^{15}N-DEST profiles (circles) and (B) ^{15}N-ΔR_2 values (filled-in circles) obtained for 300 μM (Met^{7}O)-htt^{NT} in the presence of 5 g·L^{-1} TiO_2 nanoparticles in the dark. The solid lines in (A) and open red circles in (B) represent the best-fits obtained by simultaneously fitting the relaxation data (^{15}N-DEST and ^{15}N-ΔR_2) to a three-state exchange model. The data were recorded at 600 MHz and 10 °C.

Supplementary References

1. Mudunkotuwa, I. A.; Grassian, V. H., Citric Acid Adsorption on TiO_2 Nanoparticles in Aqueous Suspensions at Acidic and Circumneutral pH: Surface Coverage, Surface Speciation, and Its Impact on Nanoparticle-Nanoparticle Interactions. *J. Am. Chem. Soc.* **2010,** *132*, 14986-14994.
2. Ceccon, A.; Schmidt, T.; Tugarinov, V.; Kotler, S. A.; Schwieters, C. D.; Clore, G. M., Interaction of Huntingtin Exon-1 Peptides with Lipid-Based Micellar Nanoparticles Probed by Solution NMR and Q-Band Pulsed EPR. *J. Am. Chem. Soc.* **2018,** *140*, 6199-6202.
3. Chen, S.; Wetzel, R., Solubilization and Disaggregation of Polyglutamine Peptides. *Protein Sci.* **2001,** *10*, 887-91.
4. Egner, T. K.; Naik, P.; Nelson, N. C.; Slowing, II; Venditti, V., Mechanistic Insight into Nanoparticle Surface Adsorption by Solution NMR Spectroscopy in an Aqueous Gel. *Angew. Chem. Int. Ed. Engl.* **2017,** *56*, 9802-9806.
5. Delaglio, F.; Grzesiek, S.; Vuister, G. W.; Zhu, G.; Pfeifer, J.; Bax, A., Nmrpipe: A Multidimensional Spectral Processing System Based on Unix Pipes. *J. Biomol. NMR* **1995,** *6*, 277-293.
6. Libich, D. S.; Fawzi, N. L.; Ying, J.; Clore, G. M., Probing the Transient Dark State of Substrate Binding to Groel by Relaxation-Based Solution Nmr. *Proc. Natl. Acad. Sci. U. S. A.* **2013,** *110*, 11361-11366.
7. Libich, D. S.; Tugarinov, V.; Clore, G. M., Intrinsic Unfoldase/Foldase Activity of the Chaperonin Groel Directly Demonstrated Using Multinuclear Relaxation-Based NMR. *Proc. Natl. Acad. Sci. U. S. A.* **2015,** *112*, 8817-8823.
8. Deshmukh, L.; Tugarinov, V.; Louis, J. M.; Clore, G. M., Binding Kinetics and Substrate Selectivity in HIV-1 Protease-Gag Interactions Probed at Atomic Resolution by Chemical Exchange Nmr. *Proc. Natl. Acad. Sci. U. S. A.* **2017,** *114*, E9855-E9862.